Experimental and Theoretical Investigation of the DC and High-Frequency Characteristics of the Negative Differential Resistance in Pseudomorphic AlGaAs/InGaAs/GaAs MODFET's

Joy Laskar, Jeffrey M. Bigelow, Jean-Pierre Leburton, *Senior Member, IEEE*, and James Kolodzey, *Senior Member, IEEE*

Abstract—**We report a detailed investigation of the negative differential resistance (NDR) in the I–V characteristics of pseudomorphic AlGaAs/InGaAs/GaAs MODFET's with gate lengths of 0.3 μm. We experimentally verify the existence of abrupt multiple NDR in both the input circuit (I_{gs} versus V_{gs}) and the output circuit (I_{gs} versus V_{gs}). The NDR occurs over a short range of drain voltage (less than 200 mV) and gate voltage (less then 5 mV) in contrast to a smooth and broader bias range (greater then 1 V) for NDR induced by thermionic emission. We provide a general interpretation of the measured dc results based on tunneling real-space transfer (TRST) which occurs because of the formation of hybrid excited states across the InGaAs channel and AlGaAs donor layer. We verify the existence of stable reflection gain in both the input and output circuits with stable broad-band frequency response in the output circuit to at least 49 GHz. These results show that NDR via TRST in pseudomorphic MODFET's can provide wide-band frequency response not limited by the electron transit time from source to drain.**

I. Introduction

THE RECENT evidence of negative differential resistance (NDR) in the drain circuit of pseudomorphic InGaAs modulation doped field-effect transistors (MODFET's) [1], [2] and GaAS/AlGaAs metal–insulator semiconductor FET's (MISFET's) [3] has shown the existence of real-space transfer (RST) [4], [5] in conventional III–V transistors. The decrease of drain current I_{ds} with increasing drain field resulting in NDR in the drain circuit of III–V FET's is accompanied by an increase in the gate current I_{gs} [1]–[3]. The increase in I_{gs} is due to a real-space transfer of electrons from the low-bandgap channel layer (either InGaAs or GaAs) to the wide-bandgap AlGaAs donor layer. It has also been established that the NDR which appears in the drain circuit can provide a high-frequency instability to 24 GHz [1], and oscillation frequency of 19.6 GHz [1], and stable wide-band reflection gain to 26.5 GHz [2]. More recently, Bigelow and Leburton [6], [7] have proposed the existence of tunneling real-square space transfer (TRST) in MODFET-like structures with NDR features similar to the experimental observations of Laskar *et al.* [2]. In addition, the negative transconductance g_m provides a mechanism by which special analog and digital functions can be implemented with reduced device count [8] including the possible implementation of complementary logic functions [9].

In this paper we present the results of further investigations of the dc and high-frequency characteristics of NDR in MODFET's. We experimentally verify the existence of abrupt multiple NDR in both the input circuit (I_{gs} versus V_{gs}) and the output circuit (I_{ds} versus V_{ds}). Theoretically, we show that the intermixing of sublevels across the InGaAs channel and AlGaAs donor layer leads to the formation of hybrid excited states causing NDR via TRST. Finally, we investigate several different modes of high-frequency operation for these MODFET's. These devices can be operated in a conventional FET manner providing cut-off frequencies greater than 100 GHz. We observe that at certain bias points near the transitions in I_{ds} no oscillations are produced over a wide frequency range, verifying the existence of stable broad-band reflection gain. In addition, the NDR produced at the gate circuit is shown to provide a narrow-band frequency gain around 28 GHz. These results show the real-space transfer via tunneling between hybrid sublevels in the channel and donor layer leads to NDR in both the input and output reflection coefficients with a frequency response of at least 49 GHz.

Manuscript received March 13, 1991; revised July 2, 1991. This work was supported by the NSF under Grants EET 87-19100 and CDR-43166, the JSEP under Contract N00014-84C-0149, and AT&T Affiliates 52. The review of the paper was arranged by Associate Editor N. Moll.

J. Laskar is with the Center for Compound Semiconductor Microelectronics and the Department of Electrical and Computer Engineering, University of Illinois at Urbana-Champaign, Urbana, IL 61801.

J. M. Bigelow and J. P. Leburton are with the Beckman Institute for Advanced Science and Technology and the Department of Electrical and Computer Engineering, University of Illinois at Urbana-Champaign, Urbana, IL 61801.

J. Kolodzey was with the Center for Compound Semiconductor Microelectronics and the Department of Electrical and Computer Engineering, University of Illinois at Urbana-Champaign, Urbana, IL 61801. He is now with the Department of Electrical Engineering, University of Delaware, Newark, DE 19716.

IEEE Log Number 9104669.

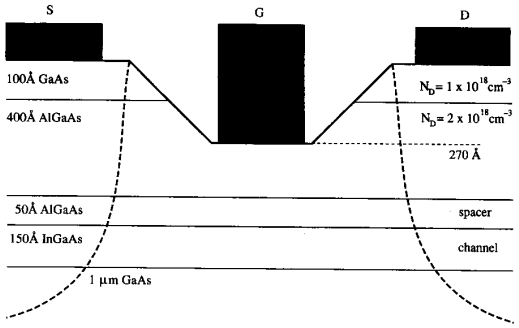

Fig. 1. Schematic diagram of the cross section of the AlGaAs/InGaAs/GaAs MODFET studied in this paper.

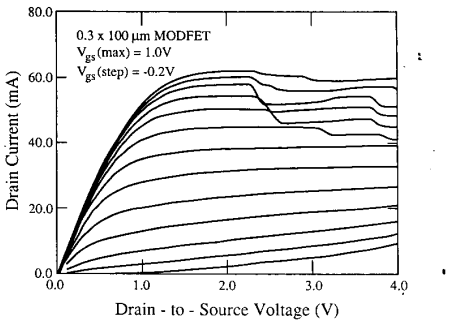

Fig. 2. Measured drain current versus V_{ds} of a MODFET exhibiting multiple NDR at 300 K with $L_g = 0.3$ μm, $W_g = 100$ μm, and $L_{sd} = 2$ μm. The maximum $V_{gs} = +1.0$ V with a step of -0.2 V.

II. DC Results

A. Experimental Investigation

The pseudomorphic MODFET's were grown by molecular beam epitaxy or semi-insulating (100) GaAs substrates. A diagram of the device structure is shown in Fig. 1. Several growth and processing runs have been performed with different indium channel compositions (15%, 17%, and 20%) and threshold voltages from -1 to 0 V. A Cambridge 6.5 EBMF electron-beam lithography system was used to fabricate devices with gate lengths of 0.3 μm having a T cross section. Device fabrication techniques are described elsewhere [10].

The dc results were obtained with an HP 4142 source/monitor unit and a Cascade coplanar waveguide probe system [11]. The devices have a ground–signal–ground layout for high-frequency measurements. The devices exhibit good pinch-off, low-output conductance, and no evidence of the so-called kink effect, which is characterized by a sharp increase in the output conductance with increasing V_{ds} [12]. We have observed pronounced NDR in the input (gate) and output (drain) circuits. The I_{ds} versus V_{ds} characteristics for a typical 0.3-μm × 50-μm pseudomorphic MODFET are shown in Fig. 2. The I–V characteristic of Fig. 2 was reproducible over many measurements scans and was observed with both digital and analog curve tracers.

There are several salient features associated with the I–V characteristics shown in Fig. 2. First, we confirm the existence of multiple NDR in the *output circuit* (drain–source characteristics). The sharp decreases in the drain current are experimentally correlated to sharp increases in the gate current. The I_{ds} transitions occur over a V_{ds} range of less than 200 mV in contrast to the relatively large transition voltages observed in [1], [3]. In general, as V_{ds} is lowered a corresponding higher V_{gs} value is required for the onset of NDR and at high enough V_{gs} we observe no NDR.

Second, we show for the first time the existence of multiple NDR in the *input circuit* (I_{ds}–V_{gs} characteristics) of these MODFET's. Typical I_{ds} versus V_{gs} and I_{gs} versus V_{gs} curves are shown in Fig. 3. The V_{gs} transition voltages occur over a range of less than 5 mV and are much smaller

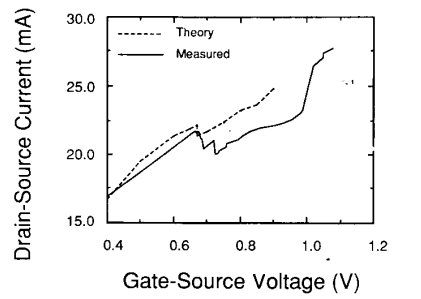

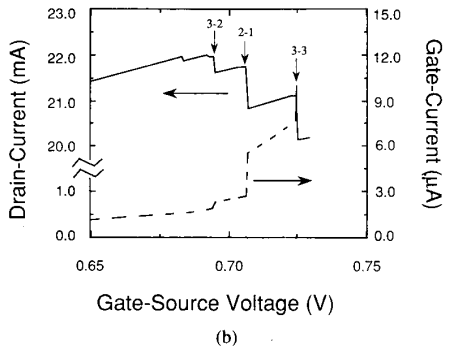

Fig. 3. (a) Measured (solid line) and simulated (dashed line) drain current versus V_{gs} of a MODFET at 300 K with $V_{ds} = 4.0$ V with $L_g = 0.3$ μm, $W_g = 50$ μm, and $L_{sd} = 3$ μm. (b) Exploded view of the measured drain current (solid line) and measured gate current (dashed line) versus V_{gs} with $V_{ds} = 4.0$ V for same device as in Fig. 3(a). The arrows with numbers refer to the different values of V_{gs} at which coupling occurs between sublevels in the InGaAs channel (first number) and AlGaAs donor layer (second number).

than transition voltages reported in previous work [1], [3]. We observe that the sudden decreases in I_{ds} versus V_{gs} for a given V_{ds} correspond to simultaneous increases in I_{gs}. Third, the existence of negative g_m is confirmed [2], although for practical applications the bias range for negative g_m should be increased. Finally, the existence of multiple NDR in the I_{ds}–V_{gs} characteristics—corresponding to multiple transition points in the I_{gs}–V_{gs} characteristics—and the relatively small-voltage bias range over which all

current transitions occur conclusively distinguishes our observations from the thermionic emission as observed in previous work.

B. Model

Tunneling real-space transfer of charge occurs when two-dimensional hot-electron states in the high-mobility MODFET channel mix with cold two-dimensional quantized states in the high-gap low-mobility AlGaAs barrier. The mixing or hybridization between barrier and channel states establishes the tunneling process producing charge transfer and inducing NDR in the device characteristics [6]. In the recessed-gate MODFET of Fig. 1, an application of V_{ds} heats up the carriers in the InGaAs channel and increases the occupation of higher energy levels. AlGaAs and InGaAs states that remain sufficiently far apart have wave functions which are localized in their respective channels. However, increasing V_{gs} has the effect of lowering sublevels and creating additional localized states in the AlGaAs layer. At certain values of V_{gs}, the AlGaAs levels cross higher InGaAs levels where they form a hybrid pair as shown in Fig. 4. Real-space transfer of charge from the high-mobility InGaAs channel to the low-mobility AlGaAs can take place and NDR is induced if enough hot electrons have been excited to the hybrid levels. In addition, the charge redistribution caused by carrier heating modifies the potential in the channel, which shifts the quantum levels and results in wave function mixing that is more sudden than in cold carrier systems [13]. The hybridization is therefore a sensitive function of voltage so that the states in the channel delocalize over a small voltage range and produce abrupt NDR. This is especially important in pseudomorphic MODFET's where there is always some conservation of the in-plane momentum due to the electron effective mass difference between AlGaAs and InGaAs. But if the wavefunctions in the transverse direction are hybridized for only a small voltage range, energy conservation permits fast elastic tunneling for these bias configurations only.

Only the source end of the channel presents conditions favorable for TRST-induced NDR to occur since the carrier loss from the InGaAs channel will determine the current, regardless of what occurs further along the channel. In addition, since the longitudinal electric field does not exceed 3 kV/cm at the source end of the channel, moderate carrier heating takes place which repopulates the InGaAs upper energy levels without inducing thermionic carrier transfer. The latter mechanism would result in a smoother NDR [1], [3] and offset TRST. Given the low value of the longitudinal field near the source end of the channel, we can apply the gradual channel approximation and look at a slice of the device in this region.

By using a charge-control model in the InGaAs channel and a velocity-field relationship given by [14]

$$v(x) = \frac{\mu_2 E(x)}{1 + \dfrac{E(x)}{E_c}} \tag{1}$$

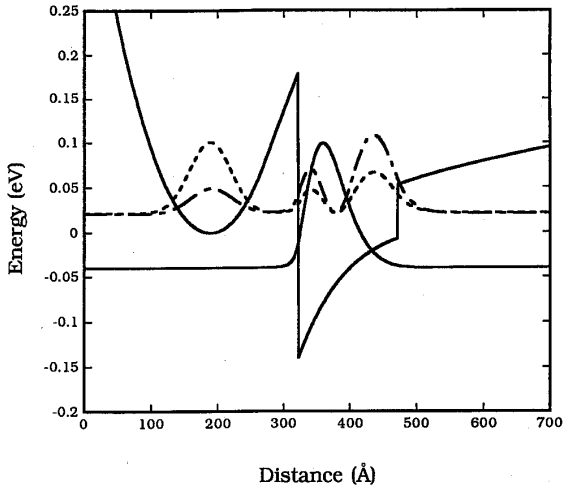

Fig. 4. Conduction-band-edge energy and wave functions squared of first three sublevels as a function of position for the MODFET of Fig. 1 for V_{gs} = 0.67 V and V_{ds} = 4.0 V. The wave functions are superimposed on the energies of the corresponding sublevels. The second (dash-dot line) and third (dashed line) sublevels are separated by only 2 meV which is barely visible on the energy scale.

the longitudinal field at the source end of the gate edge can be derived as [15]

$$E_s = \frac{E_c}{1 + \dfrac{2E_c L_{\text{eff}}(V_{ds})}{V_{gs} - V_T}} \tag{2}$$

for a device in saturation. Here μ_2 and E_c are the zero field electron mobility and the saturation field in the InGaAs, respectively. L_{eff} is the effective channel length and V_T is the threshold voltage. This simple expression for the source field shows that both V_{gs} and V_{ds} determine the longitudinal field at the source, the latter through the effective channel length L_{eff} which shrinks as V_{ds} increases when the device is in saturation.

In our model the electrons are characterized by a Fermi–Dirac energy distribution with an electron temperature T_e. The relationship between the longitudinal field and T_e is calculated with the Stratton model [16] which mainly considers polar-optic phonon scattering. We assume no more electrons are added in their respective channels as they are heated which results in a nonequilibrium situation. We calculate the quasi-Fermi level self-consistently with a Schrödinger/Poisson equation solver and find the band-edge profile and the wavefunctions in both InGaAs and AlGaAs layers. Fig. 4 shows the conduction band edge and bottom three sublevels for the bias configuration at which tunneling is predicted to occur. The wavefunctions are superimposed on the energies of the corresponding sublevels and show the mixing between the two closest levels.

In this elementary analysis of the NDR characteristics we only focus on the interaction between the lowest AlGaAs level and the first excited InGaAs level, as this crossing of levels yields the greatest occupation of elec-

trons. The device is then assumed to operate in one of two modes. In the decoupled mode there is no hybridization nor tunneling between the two levels so the carriers are characterized by two different quasi-Fermi levels on each side of the heterobarrier. In the coupled mode, electrons tunnel through the heterobarrier into the AlGaAs and relax the separation of quasi-Fermi levels. The abruptness in the current drop is due to the transition between the two modes of operation and depends upon the quasi-Fermi level separation before tunneling occurs.

The overall current is calculated from

$$I_{ds} = eW(n_1\mu_1 + n_2\mu_2)E_s \tag{3}$$

where e is the electron charge, n_1 is the electron density in the low-mobility (μ_1) AlGaAs layer, n_2 is the electron density in the high-mobility (μ_2) InGaAs layer, and W is the device width. For the simulation, we used [17], [18] $W = 50\ \mu$m, $V_T = -0.48$ V, $v_{sat} = 1.35 \times 10^7$ cm/s, $\mu_1 = 300$ cm^2/V · s, and $\mu_2 = 9160$ cm^2/V · s. From (1), $v_{sat} = \mu_2 E_c/2$, giving $E_c = 2.9$ kV/cm. L_{eff} was estimated from measured I_{ds} and V_{ds} values. From (3) it is seen that if appreciable carrier transfer between n_2 and n_1 occurs more rapidly than the increase in electric field significant NDR will occur.

C. Discussion of dc Results

The experimental and theoretical I_{ds}–V_{gs} relationships at $V_{ds} = 4.0$ V are shown in Fig. 3(a). The model predicts NDR to occur at $V_{gs} = 0.67$ V, in excellent agreement with the experimental results and supports our approach of considering only the source end of the channel. The condition for NDR is illustrated in Fig. 4 when the lowest AlGaAs level forms a hybrid pair with the first excited InGaAs level. The model also agrees with other trends seen in the I_{ds}–V_{ds} curves shown in Fig. 2. First, we see that the onset of NDR occurs at lower V_{ds} for higher V_{gs} values, since increasing V_{gs} lowers the AlGaAs level with respect to the InGaAs level and thus requires a smaller V_{ds} value to heat up and redistribute the carriers in the channel to align the sublevels. In addition, as seen in (2), increasing the gate bias increases the field near the source. Second, a threshold gate bias is necessary for the lowest AlGaAs level to cross the highest InGaAs level to induce TRST. Finally, the drop in the drain current occurs over a much smaller voltage range in the I_{ds}–V_{gs} than in the I_{ds}–V_{ds} curves because the wavefunction coupling is more sensitive to changes with the perpendicular field (V_{gs}) rather than with the longitudinal field (V_{ds}).

In our one-dimensional approximation, we have calculated the fields and gate biases necessary to create the conditions for TRST. The longitudinal field in the channel is not constant along the channel and this variation of the field needs to be taken into account in order to explain all the features of the experimental curves. In Fig. 5 we show a qualitative profile of the field along the channel for two values of gate bias V_{gs1} and V_{gs2} where $V_{gs1} < V_{gs2}$. As mentioned before, increasing the gate bias increases the field near the source. For V_{gs1}, there is a range of longitudinal electric field values for which a pair of levels are coupled together, bounded by E_1 and E_1'. Likewise, a range of fields bounded by E_2 and E_2' will couple the same two levels for V_{gs2}. Since the effect of the gate is to lower the AlGaAs level with respect to the InGaAs level, the values for the longitudinal field needed for coupling are smaller for larger gate biases. This means the position in the channel where TRST occurs for a given level crossing will move toward the source for larger gate biases, as shown in Fig. 5. Eventually, for large enough values of gate bias, the conditions for coupling cannot be met along the channel and the carriers will remain in the InGaAs channel, resulting in a switch back to the higher drain current value as seen in Fig. 3(a). These arguments also apply for constant V_{gs} and increasing V_{ds}. However, since the hybridization is more sensitive to changes in gate bias, the effects are not as evident. In Fig. 2, the increase in drain current can be seen for gate biases between 0.2 and 0.8 V for $V_{gs} \sim 3.0$ V.

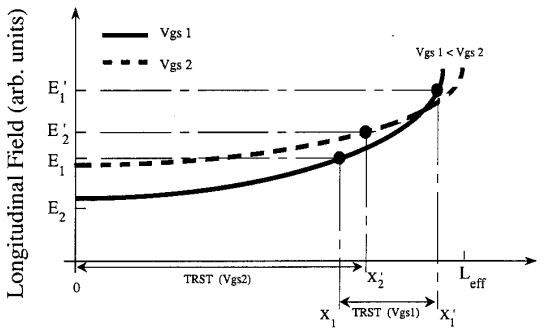

Fig. 5. Schematic representation of the longitudinal field versus position in the channel where 0 on the horizontal axis represents the source end of the channel. For applied bias V_{gs1} (solid line) coupling occurs between the longitudinal field values of E_1 and E_1' and between X_1 and X_1' in the channel denoted by TRST (V_{gs1}). When V_{gs} is increased to V_{gs2} (dashed line) coupling occurs between the longitudinal field values of E_2 and E_2' and between 0 and X_2' in the channel, denoted by TRST (V_{gs2}). As V_{gs} increases the position in the channel where TRST occurs moves towards the source.

With these considerations, the distinction between the NDR observed in the short-gate-length device [2], [4] and in devices with longer gates [1], [3] becomes more understandable. In order to maintain the same field distribution for TRST to occur in the longer gate devices, the drain–source bias would have to be increased substantially. Therefore, at the position where the field conditions for TRST are present, the potential drop in the channel is high enough for the electrons to achieve thermionic emission over the barrier and mask out the TRST.

The coupling between the first AlGaAs and second InGaAs levels is not the only occurrence of TRST. Other AlGaAs and InGaAs levels couple at different gate biases, although the effect on the current is expected to be weaker because of smaller occupation of electrons at these levels. The other couplings that create the multiple drops in current are identified in Fig. 3(b). These other couplings also create the multiple NDR observed in the I_{ds}–V_{ds} curves as

seen in Fig. 2. However, in this case, the level couplings are controlled by the heating of carriers in the channel due to the applied drain bias and have a similar behavior with field along the channel as discussed for the first AlGaAs and second InGaAs level coupling.

III. High-Frequency Results

The high-frequency results were obtained using an HP 8510B automatic vector network analyzer and a Cascade Microtech 42D probe station. The scattering (S) parameters of the MODFET were measured from 0.5 to 30.0 GHz in a coaxial 50-Ω measurement system. One port reflection measurements were made on the drain–source circuit of these devices using an external millimeter-wave U-band one-path, two-port test set. Waveguide to coaxial transitions were used to couple the high-frequency signal into wide-bandwidth millimeter-wave coplanar probe heads, providing a measurement bandwidth of 40 to 49 GHz. The electrical reference plane was established by an off-wafer short-open-load-thru calibration on an impedance standard substrate supplied with the high-frequency probe system.

In our investigation of the high-frequency performance of these MODFET's that exhibit NDR we have operated the devices in three distinct modes: 1) "conventional" III–V FET operation for peak g_m resulting in high f_T and f_{max} values, 2) stable reflection gain in the output or drain reflection coefficient (S_{22}), and 3) stable reflection gain in the input or gate reflection coefficient (S_{11}) of the device. The measured S-parameters are used to calculate both the unilateral gain (G_u) and current gain (H_{21}). Both the G_u and the H_{21} show a −6-dB/octave roll-off and the optimum value for f_{max} is ~120 GHz and for f_T is ~63 GHz, as shown in Fig. 6. There is no evidence of instability in either the input or output reflection coefficients allowing the device to be operated as a high-speed switch or microwave amplifier.

In the second mode of operation the device is biased near the first NDR point in the I_{ds}–V_{ds} characteristic for given V_{gs} values. The first issue we address is whether we can obtain stable reflection gain in the output circuit. To this end we have measured the frequencies of oscillation with a Tektronix 2755 spectrum analyzer. From the spectrum analyzer trace in Fig. 7 we see that there is a bias point at which almost no energy is detected over a wide frequency range on the spectrum analyzer resulting in stable reflection gain over a similar frequency range on the network analyzer in Fig. 8. This broad-band reflection gain has been measured to at least 49 GHz (the limit of our network analyzer), see Fig. 9, and there is no evidence of roll-off in the gain at these frequencies.

The final mode of operation is the input reflection coefficient or S_{11} versus frequency when NDR is observed in the I_{gs}–V_{gs} characteristic. The condition for NDR in the gate arises from a sharp increase in I_{ds} and corresponding decrease in I_{gs} for $V_{gs} \approx 1.0$ V in Fig. 3(a). One possible mechanism for this switching effect is the termination of tunneling between hybrid states between the donor and

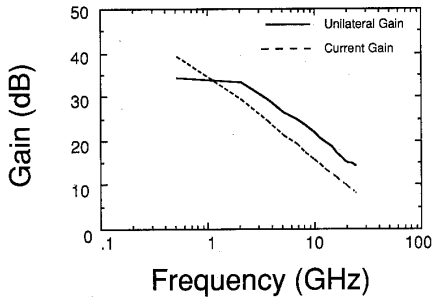

Fig. 6. Plot of the measured unilateral gain (solid line) and measured current gain (dashed line) from 0.5 to 26.5 GHz at 300 K. These results are from a 0.3 × 50 μm MODFET operated in a conventional manner with V_{ds} = 1.5 V, V_{gs} = −0.54 V, and I_{ds} = 13 mA. The gain roll-off is smooth, follows a −6-dB/octave roll-off, and is extrapolated to unity gain resulting in an f_T value (from the current gain) of 63 GHz and an f_{max} value (from the unilateral gain) of 120 GHz.

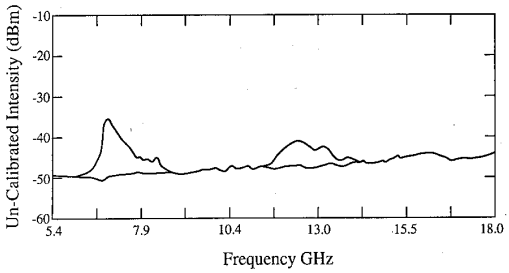

Fig. 7. Spectrum analyzer trace of a 0.3 × 50 μm MODFET showing no spontaneous oscillations over a frequency range from 5.4 to 18.0 GHz. The MODFET output circuit characteristics (drain–source) are measured with V_{gs} = 0.86 V, V_{ds} = 4.0 V, and I_{ds} = 21 mA. The reflection gain as measured on a network analyzer is stable as shown in Fig. 9.

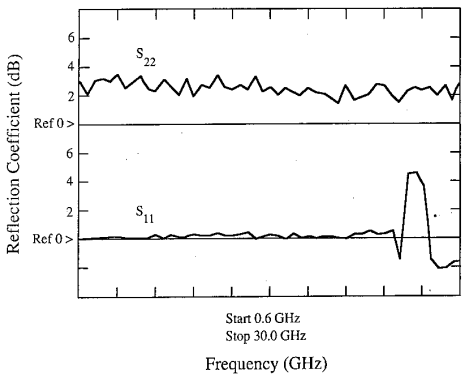

Fig. 8. Reflection coefficient of both the input characteristics $|S_{11}|$ and output characteristics $|S_{22}|$ of a 0.3 × 50 μm MODFET from 0.6 to 30 GHz with 2.94 GHz per frequency division. The bias conditions for the S_{22} trace are the same as in Fig. 9 showing a broad-band frequency response to 30 GHz which is stable as verified by the spectrum analyzer trace in Fig. 7. The bias conditions for S_{11} are V_{ds} = 3.3 V, V_{gs} = +0.73 V, and I_{ds} = 18 mA with $|S_{11}|$ = 4.6 dB at 26 GHz.

channel layers as discussed above. As we begin to apply a positive gate bias to the device with the particular I_{gs}–V_{gs} and I_{ds}–V_{gs} characteristics shown in Fig. 3 we see a stable narrow-band region of gain exists for S_{11} centered around 28 GHz as shown in Fig. 8.

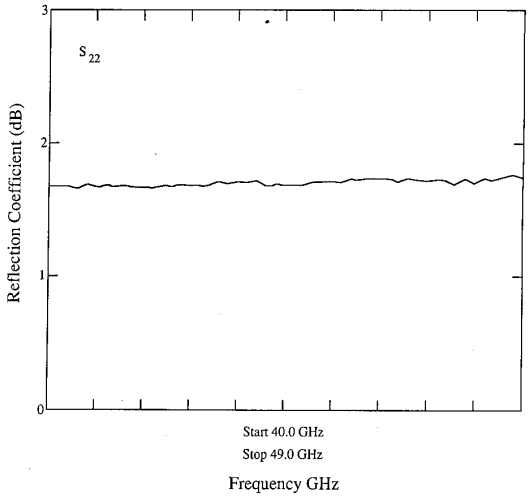

Fig. 9. Reflection coefficient $|S_{22}|$ versus frequency from 40 to 49 GHz with a frequency division of 0.9 GHz for a 0.3 × 50 μm MODFET with V_{ds} = 4.92 V, V_{gs} = 1.32 V, and I_{ds} = 32 mA. We measure a broad-band stable frequency response to 49 GHz with $|S_{22}|$ = 1.8 dB at 49 GHz with no evidence of roll-off in the reflection gain versus frequency.

There are several mechanisms which also might be expected to produce dc NDR in the drain I–V characteristic of the MODFET including: thermal heating [19], kink effect [12], and the transferred electron effect. For our observations, thermal heating can be ruled out since the drain current characteristic flattens out under higher bias conditions and does not decrease under higher power dissipation. Thermal effects will not give reflection gain [19]. The kink effect caused by deep trapping centers in the AlGaAs cannot be responsible for the NDR here since the time constant associated with trapping is large resulting in effects at relatively low frequencies below 1 GHz [20]. The abrupt decrease in I_{ds} and corresponding increase in I_{gs} indicates a sudden rise in electron flow across the hetero-interface. The high-frequency microwave signal generated by this mechanism, up to 49 GHz, proves that a high-speed mechanism is involved. The wide bandwidth of the reflection gain in the output circuit precludes impact ionization operation which produces narrow-frequency bands related to the transit time, such as in the IMPATT [19]. The narrow-band response observed in the input circuit maybe due to a combination of transit time limited operation and a different loading impedance caused by a larger gate–source impedance.

The investigation of the frequency response of this reflection gain is important since the ultimate cut-off frequency is not limited by the $f_{\max}$ value measured in a conventional FET mode which is governed by the conventional transit time $\tau = W/V$ where W is the electron transit distance and V is the electron velocity. In the NDR mode of operation the transit frequency is limited by the real-space transfer of the electrons via tunneling from the channel to the donor layer. We can estimate the characteristic tunneling time from the uncertainty principle giving $\tau_{\text{tun}} = h/2\Delta E$ [21] where ΔE is the sublevel separation. For $\Delta E \sim 3$ meV, τ_{tun} has been estimated to be less than 1 ps [6]. We have also attempted to obtain stable reflection gain at the second NDR point in the I_{ds}–V_{ds} characteristic but we have generally found that there is energy across a broad frequency range on the spectrum analyzer. We have not achieved stable gain at the higher V_{ds} values and this may partially be due to the increase of thermionic emission over the heterostructure and/or the influence of Gunn domain formation at the high fields.

Previous results with three-terminal RST, via thermionic emission, heterostructure devices have been operated in two distinct types of devices. The first type of device is the charge injection transistor (CHINT) [22] which is based on the control of charge injection of hot electrons from a channel into another conducting layer via a heating field. The CHINT has exhibited extrapolated cut-off frequencies as high as 29 GHz in the GaAs/AlGaAs material system [23] and as high as 60 GHz in the InGaAs/AlGaAs/GaAs material system [24]. The second type of device is the negative resistance transistor (NERFET) [25] which exhibits NDR in the source–drain circuit controlled by a third terminal voltage. The NERFET has exhibited a peak-to-valley ratio as large as 160 [26] and high-frequency signal to 2 GHz [27]. The high-frequency results due to TRST reported here are significant for they show that even with a basic MODFET design the possibility exists for good high-frequency performance. Further work is necessary to provide a wider transition bias range over which TRST occurs before practical applications can be realized.

IV. Summary

In summary, we have experimentally confirmed the existence of multiple abrupt NDR in both the input and output circuits of pseudomorphic InGaAs MODFET's. The NDR occurs over a small-voltage range in contrast to the NDR induced by thermionic emission. A first-order theoretical model based on TRST gives both qualitative and quantitative agreement with the measured dc results. In addition to the conventional high-frequency operation of the device we have experimentally shown that the device can provide reflection gain in both the input and output circuits. This mode of operation provides a stable broad-band frequency response in the output circuit to at least 49 GHz where the cut-off frequency is controlled by TRST and not by the electron transit time from source to drain.

Acknowledgment

The authors wish to thank A. Ketterson and I. Adesida for device processing, J. Baillargeon and K. Y. Cheng for assistance with material growth, S. Maranowski, Dr. E. Shoell and Dr. T. Hummer-Hagger for helpful discussions, and Cascade Microtech and Hewlett-Packard for equipment donations.

References

[1] Y. K. Chen, D. C. Radulescu, G. W. Wang, F. E. Najjar, and L. F. Eastman, "Observation of high-frequency high-field instability in GaAs/InGaAs/AlGaAs DH-MODFET's at K band," *IEEE Electron Device Lett.*, vol. 9, pp. 1-3, 1988.

[2] J. Laskar, A. A. Ketterson, J. N. Baillargeon, T. Brock, I. Adesida,

K. Y. Cheng, and J. Kolodzey, "Gate-controlled negative differential resistance in drain current characteristics of AlGaAs/InGaAs/GaAs pseudomorphic MODFET's," *IEEE Electron Device Lett.*, vol. 10, pp. 528–530, 1989.

[3] E. Delhaye, T. Aguila, M. Wolny, and P. Boissenot, "Circuit application of the negative differential resistances in heterojunction GaAs MISFET's," *Japan. J. Appl. Phys.*, vol. 29, pp. 236–239, 1990.

[4] K. Hess, H. Morkoç, H. Schichijo, and B. G. Streetman, "Negative differential resistance through real space electron transfer," *Appl. Phys. Lett.*, vol. 35, pp. 469–471, 1979.

[5] M. Keever, K. Hess, and M. Ludowise, "Fast switching and storage in GaAs-$Al_xGa_{1-x}As$ heterojunction layers," *IEEE Electron Device Lett.*, vol. EDL-3, pp. 297–300, 1982.

[6] J. M. Bigelow and J. P. Leburton, "Tunneling real-space transfer induced by wave function hybridization in modulation-doped heterostructures," *Appl. Phys. Lett.*, vol. 57, pp. 795–797, 1990. (In this paper the vertical scale of Fig. 2 should read eV instead of meV.)

[7] J. M. Bigelow, J. Laskar, J. Kolodzey, and J. P. Leburton, "Observation of tunneling real space transfer in pseudomorphic MODFETs at T = 300 K," to be published in *Semicond. Sci. Technol.*

[8] F. Capasso, S. Sen, A. C. Gossard, A. Huthinson, and J. H. English, "Quantum-well resonant tunneling bipolar transistor operating at room temperature," *IEEE Electron Device Lett.*, vol. EDL-7, pp. 573–576, 1986.

[9] S. Luryi, "Coherent versus incoherent resonant tunneling and implications for fast devices," *Superlattices and Microstructures*, vol. 5, pp. 375–382, 1989.

[10] A. A. Ketterson, J. Laskar, T. L. Brock, I. Adesida, J. Kolodzey, O. A. Aina, and H. Hier, "DC and RF characterization of short gate-length InGaAs/InAlAs MODFET's," *IEEE Trans. Electron Devices*, vol. 36, pp. 2361–2363, 1989.

[11] K. R. Gleason, T. M. Reeder, and E. W. Strid, "Precise MMIC parameters yielded by 18-GHz wafer probe," *MSN*, pp. 55–65, May 1983.

[12] L. F. Palmateer, P. J. Tasker, W. J. Schaff, L. D. Nguyen, and L. F. Eastman, "dc and rf measurements of the kink effect in 0.2 μm gate length AlInAs/GaInAs/InP modulation doped field-effect transistors," *Appl. Phys. Lett.*, vol. 54, p. 2139, May 1989.

[13] A. Palevski, F. Beltram, F. Capasso, L. Pfeiffer, and K. West, "Resistance resonance in coupled potential wells," *Phys. Rev. Lett.*, vol. 65, pp. 1929–1932, 1990.

[14] G. Wang and W. H. Ku, "An analytical and computer-aided model of AlGaAs/GaAs high electron mobility transistor," *IEEE Trans. Electron Devices*, vol. ED-33, pp. 657–663, 1986.

[15] See, e.g., R. S. Muller and T. I. Kamins, *Device Electronics for Integrated Circuits*, 2nd ed. New York: Wiley, 1986.

[16] See, e.g., S. Adachi, "GaAs, AlAs, and $Al_xGa_{1-x}As$: material parameters for use in research and device applications," *J. Appl. Phys.*, vol. 58, pp. R1–R29, 1985.

[17] J. Dickmann, C. H. Heedt, and H. Daembkes, "Determination of the electron saturation velocity is pseudomorphic $Al_xGa_{1-x}As/In_yGa_{1-y}As$ MODFET's at 300 and 100 K," *IEEE Trans. Electron Devices*, vol. 36, pp. 2315–2319, 1989.

[18] T. Wang and C. Hsieh, "Numerical analysis of nonequilibrium electron transport in AlGaAs/InGaAs/GaAs pseudomorphic MODFET's," *IEEE Trans. Electron Device*, vol. 37, pp. 1930–1938, 1990.

[19] See, e.g., S. M. Sze, *Physics of Semiconductor Devices*, 2nd ed. New York: Wiley, 1981, pp. 96 and 577.

[20] A. G. Milnes, *Deep Impurities in Semiconductors*. New York: Wiley-Interscience, 1973, p. 333.

[21] T. C. L. G. Sollner, W. D. Goodhue, P. E. Tannenwald, C. C. Parker, and D. D. Peck, "Resonant tunneling through quantum wells at frequencies up to 2.5 THz," *Appl. Phys. Lett.*, vol. 43, pp. 588–590, 1983.

[22] S. Luryi, A. Kastalsky, A. C. Gossard, and R. H. Hendel, "Charge injection transistor based on real-space hot-electron transfer," *IEEE Trans. Electron Devices*, vol. ED-31, pp. 832–839, 1984.

[23] A. Kastalsky, J. H. Abeles, R. Bhat, W. K. Chan, and M. A. Koza, "High-frequency amplification and generation in charge injection devices," *Appl. Phys. Lett.*, vol. 48, pp. 71–73, 1986.

[24] M. R. Hueschen, N. Moll, and A. Fischer-Colbie, "Improved microwave performance in transistor based on real space electron transfer," *Appl. Phys. Lett.*, vol. 57, pp. 386–388, 1990.

[25] A. Kastalsky and S. Luryi, "Novel real-space hot-electron transfer devices," *IEEE Electron Device Lett.*, vol. EDL-4, pp. 334–336, 1983.

[26] A. A. Grinberg, A. Kastalsky, and S. Luryi, "Theory of hot-electron injection in CHINT/NERFET devices," *IEEE Trans. Electron Devices*, vol. ED-34, pp. 409–419, 1987.

[27] A. Kastalsky, R. A. Kiehl, S. Luryi, A. C. Gossard, and R. H Hendel, "Microwave generation in the NERFET," *IEEE Electron Device Lett.*, vol. EDL-5, pp. 321–323, 1984.

*

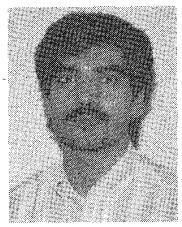

Joy Laskar received the B.S. degree with highest honors in computer engineering from Clemson University, Clemson, SC, in 1986, the M.S. degree in electrical engineering from the University of Illinois, Urbana, IL, in 1989, and the Ph.D. degree in electrical engineering also from the University of Illinois in 1991.

From 1985 to 1986 he was employed at IBM's Thomas J. Watson Research Center, Yorktown Heights, NY, in the advanced submicrometer CMOS group. He is currently a Visiting Assistant Professor in Electrical Engineering at the University of Illinois where he is part of the High Frequency Devices and IC Group. His research has centered on the characteristics of heterostructure transistors at microwave frequencies and cryogenic temperatures.

*

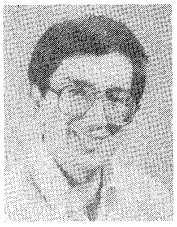

Jeffrey M. Bigelow received the B.S. degree in electrical engineering from Colorado State University, Fort Collins, CO, in 1986 and the M.S. degree in electrical engineering from the University of Illinois, Urbana, IL, in 1988. He is currently working on his Ph.D. degree in electrical engineering at the University of Illinois where he is part of the Computational Electronics Group. His work has been centered on the study and simulation of tunneling in confined heterostructure devices.

*

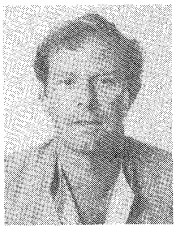

Jean-Pierre Leburton (M'83–SM'89) was born in Liége, Belgium, in 1949. He received the Ph.D. degree from the University of Liége, Belgium, in 1978.

After receiving his degree, he joined the Siemens Research Laboratory in Munich, West Germany, to work on modeling of hot-electron effects in short-channel MOS transistors. In 1981 he was a Visiting Research Assistant Professor with the University of Illinois at Urbana-Champaign, where is he now a Professor of Electrical and Computer Engineering. His research work is on the theory and modeling of semiconductor devices. He is currently interested in transport and optical properties of III–V compounds, quantum-well structures and low-dimensional systems. He has organized or co-organized several symposiums and workshops in these fields and has published about 70 technical papers in various international journals.

*

James Kolodzey (S'72–M'74–SM'90) was born in Philadelphia, PA, in 1950. He received the B.S. degree with honors in engineering physics from Lehigh University, Bethlehem, PA, in 1972, and the Ph.D. degree in electrical engineering from Princeton University, Princeton NJ, in 1986 for research on amorphous SiGe superlattices and solar cells.

From 1974 through 1982 he was employed at IBM Corp. Poughkeepsie, NY, Optical Information Systems (now the Opto-Electronics Center for McDonnell-Douglas), Elmsford, NY, and Cray Research, Chippewa Falls, WI. While in industry, he worked on optical communication and GaAs circuit design. In 1986 he joined the Department of Electrical and Computer Engineering, University of Illinois at Urbana-Champaign, as an Assistant Professor where he worked on molecular beam epitaxy, and on the characteristics of semiconductor devices at microwave frequencies and cryogenic temperatures. In 1987 he went on leave to work on molecular beam epitaxy with Dr. A. Y. Cho at AT&T Bell Labs, Murray Hill, NJ, and in 1990 he went on leave to work on SiC superlattices with Drs. F. Koch and R. Schwarz at the Technical University of Munich, Munich, FRG. In 1991 he joined the facility of the University of Delaware, Newark, where he is an Associate Professor of Electrical Engineering. His research centers on high-frequency measurements of materials and devices, molecular beam epitaxy of group IV compounds, and integrated optoelectronics.